Journal of Imaging Science and Technology® 57(5): 050503-1–050503-15, 2013.

Geometry-Independent Target-Based Camera Colorimetric Characterization

Farhad Moghareh Abed and Roy S. Berns▲
Munsell Color Science Laboratory, Rochester Institute of Technology, Rochester, 14623, NY
E-mail: fxa6577@rit.edu

Kenichiro Masaoka
NHK Science & Technology Research Laboratories 1-10-11 Kinuta, Setagaya, Tokyo 157-8510, Japan

Abstract. *An accurate colorimetric characterization of digital still cameras (DSCs) is vital to any high-quality color-reproduction system. However, achieving a perfect relationship between DSC responses and input spectral radiance is not practically easy, even when they have a reasonable linear relationship. In this research, we investigated differences in capturing geometries as a source of nonlinearity in camera characterization workflows. This nonlinearity can be corrected using a physical model describing the spectrophotometric changes according to illumination/capturing geometries. We introduced a model based on the Saunderson equation as an approach to predict surface properties suitable for paint layers in different geometries. According to the results, the Saunderson surface correction successfully compensated for the dissimilarities among spectrophotometric and spectroradiometric measurements, regardless of the capturing and lighting geometries. The model was also used for characterizing digital still cameras using matte, semi-glossy and glossy color targets as training datasets. The Saunderson-based models improved the transformation matrix for different geometries compared to conventional methods. Also, the results confirmed the validity of a simpler derivation of the Saunderson surface correction based on linear matrix operations.* © *2013 Society for Imaging Science and Technology.*
[DOI: 10.2352/J.ImagingSci.Technol.2013.57.5.050503]

INTRODUCTION

Having an accurate image acquisition system is imperative for any high-quality color management workflow, influencing the error cascading through the whole system. Besides the capacities of image-capturing hardware, color characterization techniques can be a significant source of error in the acquisition steps. For digital still cameras (DSCs), color characterization methods refer to the techniques of converting camera responses (e.g. RGB) to a device-independent colorimetric representation (e.g. CIEXYZ).[1–4] The capability of current DSCs in high-quality and reliable image acquisitions has generated the interest of using such instruments as image-based (two-dimensional) colorimeters in scientific applications. Basically, the constitutive optical elements of DSCs and scientific colorimeters are fundamentally identical. In addition, the availability of RAW data from current DSCs removes any extra and unwanted processes (e.g., white balance and gamma correction), providing more flexibility for accurate color characterizations.

The target-based color characterization of DSCs has been the subject of many research articles in the past decade,[5–13] evaluating a number of factors affecting the accuracy of color characterization regarding utilized characterization algorithms, color target structure, and camera hardware. The conclusions mostly point out that the target-based characterization methods are valid for a particular lighting geometry, color target materials, and surface structure. This dependence had led to designing optimized color targets in recent research, taking into account several factors, such as material, gamut, and the number of color patches, with less consideration of the role of lighting geometry on the color target appearance. The variety of capturing geometries and the uncontrolled nature thereof are other factors increasing the complexity of the characterization process. The more divergent these geometries and differences in surface properties between the profiling target and object, the greater the characterization error. To avoid possible appearance changes caused by the capturing geometries, it is recommended to keep the viewing/illuminating geometry consistent with the measurement geometry and typical observing conditions.[1,2,5] The material aspects become important particularly when color patches vary in surface and spectral properties, leading to different appearance changes according to geometry changes. On the other hand, DSCs have the potential of acting as colorimeters independent of any geometrical capturing structure and color target materials. In this research, we investigated the dependence of target-based camera color characterization with respect to the target's surface structure and camera-taking geometry. It will be discussed that this dependence on capturing conditions can be predicted and in turn reduced by compensating for geometry and surface characteristics using an appropriate optical model.

THEORY

Color characterization for DSCs provides the relationship between an device-dependent (e.g. RGB) and a device-independent (e.g. CIEXYZ) color spaces. Basically, color characterization methods are divided into two general

▲ IS&T Member.

Received Jan. 7, 2013; accepted for publication Aug. 15, 2013; published online Sep. 1, 2013. Associate Editor: Jon Yngve Hardeberg.
1062-3701/2013/57(5)/050503/15/$20.00

categories in the literature: spectral sensitivity-based ones, and color target-based ones, as specified by ISO17321.[14] The spectral sensitivity-based models connect device-dependent and device-independent color spaces by a linear combination of camera spectral sensitivity curves and color matching functions.[5,8,9,14–16] In the target-based characterization method, this relationship is established according to a set of color patches with available pre-measured spectral or colorimetric data. The concepts investigated in this research mostly include the target-based DSC characterization method since it is inexpensive and more practical compared to the other method. Nevertheless, other device characterization methods, including spectral sensitivity-based techniques and those for characterizing scanners, can still benefit from the conclusions drawn in this research.

The simple polynomial-based regression methods have been introduced as practical and simple models with satisfactory accuracy compared to other methods. In most of the proposed methods, camera responses are required to be RAW data and already corrected for nonlinearity, dark current, and optical flare. In many cases, a simple linear transformation is sufficient to map device-dependent and device-independent spaces with adequate performance; even so, higher-order polynomials have reportedly improved estimations.[5] It is also mentioned that the lower-order conversions are preferred to avoid unwanted local maxima and minima in the transformation, as well as over-fitting systematic errors, which cause dependence on specific capturing conditions.[1,2] As a conclusion, even though a simple linear mapping seems to be sufficient, it is not perfectly achievable in practice.

Another disadvantage of target-based characterization methods is a higher risk of dependence on a particular lighting/illumination geometry and training color target materials. Hence, it is recommended to restrict the acquisition geometry corresponding to spectrophotometric measurements in high-quality color-capturing systems. For instance, the capturing geometry recommended by ISO17321 contains two equally spaced illumination sources with a 45° incident angle to the center of the target area. The DSC is placed normal to the test target to prevent specular reflections. The characterization matrix provides accurate data to the extent that the geometry of spectral and camera-capturing measurements are matched.

We will discuss that some of the current characterization limitations are due to the differences of the lighting/viewing geometries influencing the material appearances. For example, matte and glossy surfaces appear differently in a 45°:0° geometry despite similar reflectance factor when measured by a d:0° spectrophotometer. Two objects may have a similar reflectance factor for a particular viewing geometry, but differ for other lighting conditions. As a result, further information, i.e., either surface characteristics or the geometrical conditions, should be expressed in addition to the spectral data for a more comprehensive description of the surface characteristics. In other words, the reflectance factor of any surface varies with respect to the light incident and detecting angles.

The reflectance factor is defined as *the ratio of the radiant or luminous flux reflected in the directions delimited by the given cone to that reflected in the same direction by a perfect reflecting diffuser identically irradiated or illuminated*.[17] This quantity is calculated based on the sensor response by knowing the radiant flux received from the surface relative to a reference white after dark current subtraction.[18] The workflow is almost the same for colorimeters, except that the amount of energy is integrated along visible wavelengths weighted by color matching functions. Similar to reflectance factors, colorimetric measurements also can be varied depending on the capturing geometry. In a typical target-based camera characterization, camera signals are related to the colorimetric values corresponding to a specific spectrophotometer geometry that might not be matched to the camera-taking geometry. This mismatch is already mentioned by some researchers as a possible source of error, but without proposing any practical solutions.[2,19] Ideally, the actual radiant flux of the measurement in the scene must have a perfect correlation with the linearized camera signals where camera RGB sensitivity functions span human eye color matching functions properly. In such cases, the DSC is independent of the training material and capturing geometry, since it simply converts the camera responses to the corresponding relative radiant flux similar to a colorimeter. Illumination/capturing geometry mismatches can be a source of a disagreement between spectral measurements and camera responses during the characterization procedure. Appropriate corrections should be embedded within the characterization procedure when the geometric differences are noticeable. This consideration needs a model for describing the surface properties in a variety of illumination/capturing conditions such as the bidirectional reflectance distribution function (BRDF). The BRDF provides a comprehensive description of material surfaces for all possible incident and reflected geometries.[20] BRDF-based methods, however, require precise knowledge of the capturing geometry as well as complex instrumentation. In most cases, none of the mentioned requirements are easily accessible. On the other hand, the color targets for camera characterization typically have isotropic uniform surfaces, which can be described by simpler surface correction methods, such as the Ward model[21] or the Saunderson equation.[22,23] The Saunderson correction is commonly used in colorant formulation, accounting for spectrophotometer geometry. In this research, we have selected the Saunderson equation as a simple surface correction model for spectral estimations accounting for geometry differences.

The Saunderson correction relates the internal and external reflections due to changes in the refractive index at the surface of a paint layer. The equation corrects the *measured reflectance*, R_m, for surface reflections. The corrected reflectance is called *internal reflectance*, R_i, which is independent of the surface structure. The original equation was derived by Ryde for the general form of incident light

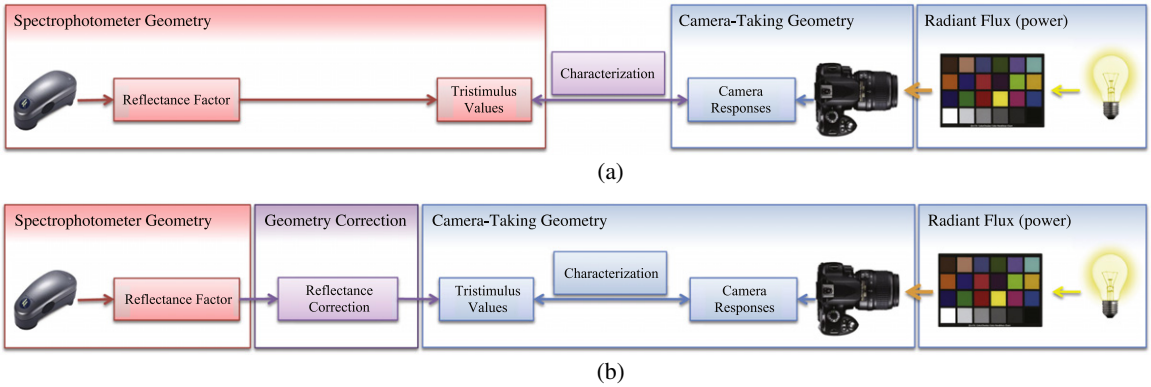

Figure 1. The characterization workflow for a typical method (a) and for the proposed (b) method.

and translucent materials.[24] Later, Saunderson applied the Ryde correction equation for color formulation of opaque pigmented plastics using Kubelka–Munk's theory. The correction equation is named after the Saunderson because of the application of the simplified equation in industry.[22–24] The general form of the Saunderson correction interrelating internal and external reflectance factor is shown in Eqs. (1) and (2):

$$R_m = \frac{(1-k_1)\,(1-k_2)R_i}{1-k_2R_i} + k_{ins}k_1 \tag{1}$$

$$R_i = \frac{R_m - k_{ins}k_1}{(1-k_1)(1-k_2) + k_2R_m - k_{ins}k_1k_2}. \tag{2}$$

The variables k_1 and k_2 are wavelength-dependent coefficients specifying the reflection portion at the surface for light incident from outside and inside, respectively. However, these values are assumed to be constant in all the visible wavelengths in most cases, including in this research. The Saunderson coefficients have already been calculated and optimized for specific measurement geometries, materials, and incident light angles, according to available spectrophotometer geometries.[22,25,26] k_1 is specified using the Fresnel equation as a function of incident angle and refractive index of the surface, suggested to be set to 0.040 for parallel light and 0° incident angle and 0.092 for diffuse lighting geometries (for a medium with refractive index of about 1.5). k_2 is usually determined experimentally, because most materials are not perfect isotropic scatterers, and it is difficult to have an accurate description of the internal specular reflectance within the pigmented layers.[25] The recommended values for paint layers varies between 0.4 and 0.6 according to the refractive index, surface properties, and the lighting geometry.[22,23] k_{ins} describes the geometry of the measurement determining the proportion of the external reflected light received by the detector. It is important to note that the Saunderson coefficients (k_1, k_2, and k_{ins}) change according to the lighting and measurement geometries. Accurate calculation of the coefficients is not always practical, even for a particular spectrophotometer with known geometry. Hence, it is recommended to apply an additional optimization algorithm to achieve the best

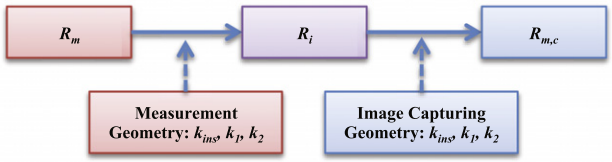

Figure 2. The workflow of correcting the measured reflectance for different geometries.

quantities.[18] The Saunderson equation can be applied in the same manner when DSCs are the measurement devices. The correction imposes the difference between the spectral radiance reaching the camera and the spectrophotometer detectors. Looking at Eqs. (1) and (2), the Saunderson equation is a function of three coefficients, which makes the model simple and easy to implement.

The main difference between a conventional and the surface-corrected method is illustrated in Figure 1. In conventional characterization methods (Fig. 1(a)), camera signals are converted to the tristimulus values of a specific spectrophotometer. Notice that the characterization algorithm connects two different geometries. Hence, camera responses and tristimulus values do not correspond to the same geometrical domain. In contrast, in the proposed method (Fig. 1(b)), the reflectance factors of the color targets are corrected, corresponding to the camera-taking geometry. Thus, the characterization algorithm directly transforms the camera responses to colorimetric values with the same geometry.

Figure 2 is a flowchart of the process of the proposed reflectance correction. The reflectance factor from the spectrophotometer, R_m, is converted to internal reflectance, R_i, using Eq. (1) and according to the geometry of the spectrophotometer. Afterward, the internal reflectance is converted to the reflectance factor of the geometry of the camera-taking system, $R_{m,c}$. In fact, the whole process is a model for characterizing the surface property that converts the reflectance factor among different illumination/capturing geometries. By a simple replacement of R_m with new coefficients in Eq. (2), reflectance values for the second geometry ($R_{m,c}$) can be calculated using a single

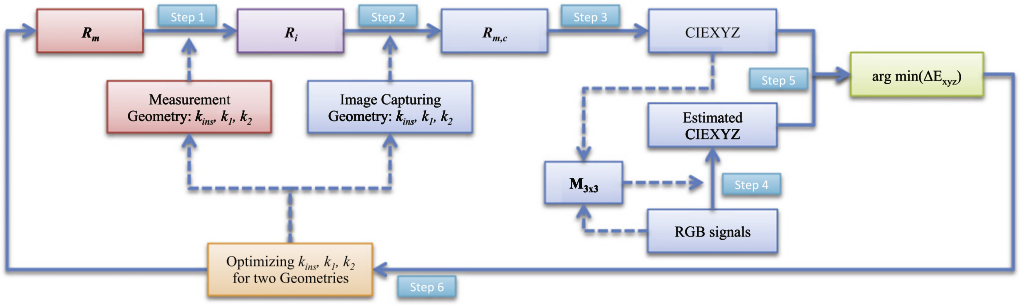

Figure 3. The workflow of optimizing Saunderson coefficients for camera profiling.

equation:

$$R_{m,c} = \frac{(1-k_1)(1-k_2)(R_m - k'_{ins}k'_1)}{(1-k'_1)(1-k'_2) - k'_{ins}k'_1k'_2 + k'_{ins}k'_1k_2 + R_m(k_2 - k'_2) + k_{ins}k_1}. \quad (3)$$

In this equation, k'_1, k'_2, k'_{ins} are the Saunderson coefficients corresponding to the second (or camera-taking) capturing geometry. Since the capturing geometry is not accurately known for the image-capturing system, the Saunderson coefficients are determined using an iteration loop to achieve the best possible linearity between DSC responses and tristimulus values after surface correction.

It should be remembered that the camera signals must already be corrected for dark current, optical flare, and linearization so that the actual entrance radiance is represented as a linear combination of the output signals (or camera responses).[1,2,4,9] Nonlinearity of two spaces can be resolved by replacing the linear equation by nonlinear ones, such as polynomial or root-polynomial equations.[27] The optimization process is illustrated in Figure 3. The measured reflectance, R_m, of the color target is converted to the internal reflectance, R_i, using the Saunderson coefficients according to Eq. (1) (step 1). Then, the calculated internal reflectance is converted back to the reflectance factor, $R_{m,c}$, but according the new Saunderson coefficients and Eq. (2) (step 2). Next, CIEXYZ values of the patches are obtained based on corrected reflectances (step 3). These two steps also can be merged as a single procedure by utilizing Eq. (3). Afterward, the camera system is characterized using the calculated CIEXYZ values and camera signals from a simple 3 × 3 matrix (step 4). The estimated and calculated CIEXYZ values are compared by a color difference formula (step 5). Any color difference formula can be considered for optimization. We used ΔE_{xyz} rather than any perceptual color difference formula to avoid any additional nonlinearity between radiance values and camera responses so a simple matrix operation could be employed. The optimization algorithm minimizes ΔE_{xyz} to reach the optimized Saunderson coefficients (step 6). Recommended coefficients in the literature are good candidates for the starting values of the optimization iteration loop.[22,26,28]

It must be remembered that the optimized coefficients (k_1, k_2, k_{ins}, k'_1, k'_2, k'_{ins}) are relative values with no physical meaning, because different Saunderson coefficients can produce identical results. The reason is that only three coefficients (rather than six) are sufficient to optimize Eq. (3). Mathematically, Eq. (3) can be written in a simpler form as a function of three variables, as shown in Appendix A:

$$R'_m = \frac{R_m + \alpha}{\beta R_m + \gamma}, \quad (4)$$

where coefficients α, β, and γ are functions of the Saunderson coefficients for both measuring and capturing geometries. As a result, using the equation with six variables (k_1, k_2, k_{ins}, k'_1, k'_2, k'_{ins}) leads to an ill-posed system of equations. One alternative to converge the coefficients to feasible values is to fix the first Saunderson coefficients (the three variables k_1, k_2, and k_{ins}) to predefined values for the utilized spectrophotometer with a known geometry.

More simplifications can be made with respect to physical facts. As an example, Eq. (3) can be expressed in a simpler form by considering the physical facts about the internal reflectance within the paint surface. The internal reflectance (k_2 and k'_2) is assumed identical for isotropic pigmented layers because the incident light will be diffused similarly inside the paint layers independent of the light incident angle. This assumption leads to a simpler form of the equation, with only two free variables (more details are provided in Appendix B):

$$R_{m,c} = \mu R_m + \rho. \quad (5)$$

Coefficients μ and ρ are also functions of the Saunderson coefficients.

Finally, the optimized Saunderson coefficients are used for calculating corrected reflectances used for deriving a 3 × 3 matrix for camera characterization by common regression algorithms or a pseudo-inverse matrix technique. It is worthwhile noting that this process can be included in common camera profiling without any necessity of further information or measurements. This simplification enables us to apply the surface corrections in colorimetric coordinates rather than spectral space.

Considering Eq. (5), spectral curves of different geometries are interrelated by a linear relationship. This linearity brings up the idea of utilizing simple matrix algebra in the colorimetric domain rather than nonlinear optimizations in the spectral domain. In this section, we proceed to

implement a method for optimizing these coefficients using matrix operations.

A typical 3 × 4 transformation matrix that maps camera responses to CIEXYZ tristimulus values of the spectrophotometer can be easily obtained by the equations below:

$$\begin{bmatrix} X_m \\ Y_m \\ Z_m \end{bmatrix} = \boldsymbol{M}_{3*4} \begin{bmatrix} R \\ G \\ B \\ 1 \end{bmatrix}, \tag{6}$$

where subscript m denotes the tristimulus values calculated from spectrophotometer spectral measurements. R, G, and B values refer to dark current subtracted and linearized camera responses. This equation is analogous to the following equation mathematically:

$$\begin{bmatrix} X_m + X_g \\ Y_m + Y_g \\ Z_m + Z_g \end{bmatrix} = \boldsymbol{M}'_{3*3} \begin{bmatrix} R \\ G \\ B \end{bmatrix}. \tag{7}$$

Here $M'_{3\times3}$ is the same matrix as $\boldsymbol{M}_{3\times4}$, except for omitting the offset column and expressing the offsets by X_g, Y_g, and Z_g values on the other side of the equation. By multiplying both sides of the equation to a scalar μ,

$$\begin{bmatrix} \mu X_m + \mu X_g \\ \mu Y_m + \mu Y_g \\ \mu Z_m + \mu Z_g \end{bmatrix} = \mu \boldsymbol{M}'_{3*3} \begin{bmatrix} R \\ G \\ B \end{bmatrix}. \tag{8}$$

Finally, by replacing X_g, Y_g, and Z_g with a set of new variables X_ρ, Y_ρ, and Z_ρ, the following equation is derived:

$$\begin{bmatrix} \mu X_m + X_\rho \\ \mu Y_m + Y_\rho \\ \mu Z_m + Z_\rho \end{bmatrix} = \mu \boldsymbol{M}'_{3*3} \begin{bmatrix} R \\ G \\ B \end{bmatrix}. \tag{9}$$

In this equation, X_ρ, Y_ρ, and Z_ρ are offset values, which are basically corresponding to the offset tristimulus values in Eq. (5) (ρ). Similarly, the tristimulus values calculated on the left-hand side of the equation are the tristimulus values of the camera-taking geometry ($X_{m,c}$, $Y_{m,c}$, $Z_{m,c}$):

$$\begin{bmatrix} \mu X_m + X_\rho \\ \mu Y_m + Y_\rho \\ \mu Z_m + Z_\rho \end{bmatrix} = \begin{bmatrix} X_{m,c} \\ Y_{m,c} \\ Z_{m,c} \end{bmatrix}. \tag{10}$$

Therefore, the transformation matrix can be simplified as follows:

$$\begin{bmatrix} X_{m,c} \\ Y_{m,c} \\ Z_{m,c} \end{bmatrix} = \mu \boldsymbol{M}'_{3*3} \begin{bmatrix} R \\ G \\ B \end{bmatrix}. \tag{11}$$

In the same manner, $X_{m,c}$, $Y_{m,c}$, and $Z_{m,c}$ are associated with the tristimulus values of $R_{m,c}$ in Eq. (5). The only unknown variable in Eq. (11) is the scalar μ. This variable can be specified by using the RGB and $XYZ_{m,c}$ coordinates of a white reference such as polytetrafluoroethylene (PTFE) as a sample with known stimuli. Dark current/flare-subtracted RGB values of PTFE are already available by the camera measurements and its XYZ values are equivalent to those of the chosen light source (XYZ_{il}), since PTFE was used for calibration. Consequently, the scaling factor, μ, can be calculated by a regression technique:

$$\mu = \left(\boldsymbol{M}'_{3*3} \begin{bmatrix} R_{PTFE} \\ G_{PTFE} \\ B_{PTFE} \end{bmatrix}_{3*1} \right)^{+} \begin{bmatrix} X_{il} \\ Y_{il} \\ Z_{il} \end{bmatrix}_{3*1}. \tag{12}$$

In this equation, the superscript + represent the matrix pseudo-inverse. The scalar is embedded within the final matrix ($\boldsymbol{M}_{cr}$) as the last step:

$$\boldsymbol{M}_{cr} = \mu \boldsymbol{M}'_{3*3}. \tag{13}$$

The normalized 3 × 3 transformation matrix ($\boldsymbol{M}_{cr}$) is used for the final camera characterization to map camera RGB space to CIEXYZ space. It must be noted that this simplification relies on the validity of the simplification regarding the internal reflectances for paint layers, which is studied in this publication. A practical procedure of this method is also provided in Appendix C.

EXPERIMENTAL

Experiments were conducted in three phases. In the first phase, the general idea of surface correction using the Saunderson equation was evaluated. The second phase of the experiment includes characterizing a digital camera using different algorithms. In the third phase of the experiment, the independence of the characterization model was studied, where the characterization procedure was applied for a dissimilar illumination geometry and color patches with different surface properties.

Phase I

The reflectance factors of a set of gray patches were measured by two spectrophotometers and a tele-spectroradiometer. A Photo Research PR-655 SpectroScan tele-spectroradiometer (PR-655) was used for the radiance measurements. The Xrite Eye-one with 45°a:0° geometry and Color-Eye 7000 with di:8° and de:8° geometries were used for spectrophotometric measurements. The set of gray patches was made by mixing different concentrations of matte (carbon black and titanium white of GOLDEN Matte Fluid Acrylic paints) and glossy (black and white paints of Sherwin Williams Acrylic high-gloss latex paints) paints. The gray scale contains 14 patches with the glossy and the matte gray surfaces, shown in Figure 4. The gray patches were approximately spectrally nonselective so as to be insensitive to the errors of wavelength misalignments and bandwidth differences between the spectrophotometers and the spectroradiometer. When the PR-655 was used, the reflectance factor of each sample

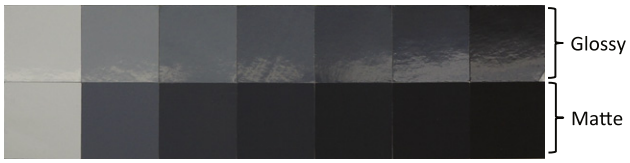

Figure 4. Gray scale with 14 glossy, matte, and semi-glossy patches.

was extracted using pressed PTFE as a reference white. PTFE has a reflectance factor of almost 1 in all visible wavelengths, and a matte surface close to a Lambertian surface. The measurements were conducted for three different lighting and capturing geometries, as shown in Figure 5. The spectral properties of the patches were the average of at least three measurements to reduce the noise, particularly for dark samples.

In the first geometry, the target was imaged under a GTI EVS light booth with a diffuse fluorescent simulated D50 lighting (Fig. 5(a)). In order to achieve a constant lighting and capturing geometry, the position of the PR-655 was kept fixed and each sample was repositioned.

In the second geometry, two directional lights (Buhlite Soft Cube light Sc-150) at almost 45° from the normal were used for illumination (45°/0°-dual-light geometry). The spectroradiometer was placed approximately at the normal axis of the target surface (Fig. 5(b)). This geometry fit the best with the proposed geometry recommended by ISO17321 (Section 4.3.3) for target-based illumination geometry.[14] The third geometry is similar to the previous one, but using only one light at 45° to the surface normal, as shown in Fig. 5(c) (45°/0°-single-light geometry). Four methods were used for geometrical compensations: (a) the *Saunderson correction*, corresponding to Eq. (3) or Eq. (4); (b) *scaler-offset*, referring to a simplified Saunderson correction as defined by Eq. (5); (c) *scaler*; and (d) *offset*, which consider a single scaler and a single offset, correspondingly. The results were compared to a case in which no correction was applied to the reflectance factors as a metric of geometrical effects on the measured spectrals. Minimizing the spectral RMS values between the spectroradiometer and spectrophotometers measurements, the coefficients of each method were optimized. Figure 6 is a plot of the optimization process. In all of the experimental phases, a nonlinear iterative optimization algorithm based on quadratic programming (the *fmincon* function in Matlab)

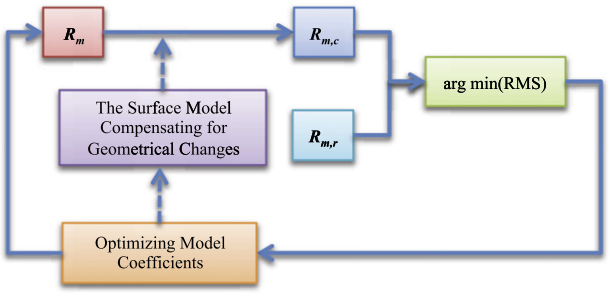

Figure 6. The workflow of optimizing the model coefficients by minimizing the spectral RMS values.

was used. The Saunderson coefficients were constrained to be between zero and unity so that they had physical meaning. Optimization iteration rapidly converged to the optimum values for all of the geometries and different initial values. If all six Saunderson coefficients were optimized, the coefficients would depend on the initial values, even though this did not affect the final error.

Results of Phase I

The RMS values between the reflectance factors measured by the two spectrophotometers and the spectroradiometer for the first phase are compared in Figure 7. As explained above, this phase includes spectral matches of glossy and matte samples in three spectrophotometric and three spectroradiometric geometries. When no correction was applied to the reflectance factors (plotted as not corrected bars in Fig. 7), the differences are extensive, highlighting that the geometrical changes do influence the measured reflectance factor as expected. The more the geometrical dissimilarities, the larger the spectral differences. For instance, reflectance factors measured by the Color-Eye 7000 di:8° have the largest RMS values compared to reflectances measured by the PR-655 with the 45°/0°-single-light geometry. On the other hand, the Eye-one spectrophotometer produced a good correlation with the 45°/0°-dual lights (which is a symmetrical directional lighting geometry) since they have analogous lighting and capturing characteristics. Thus, selecting spectrophotometers in accordance with the capturing geometries reduces spectral errors. The measurement geometry using an integrating sphere and specular excluded (de:8°) resulted in smaller RMS values compared to specular included (di:8°)

(a) (b) (c)

Figure 5. Lighting and capturing setups for measuring the spectral radiance by the PR-655. (a) Diffuse lighting, (b) 45°/0°-dual lights, (c) 45°/0°-single light.

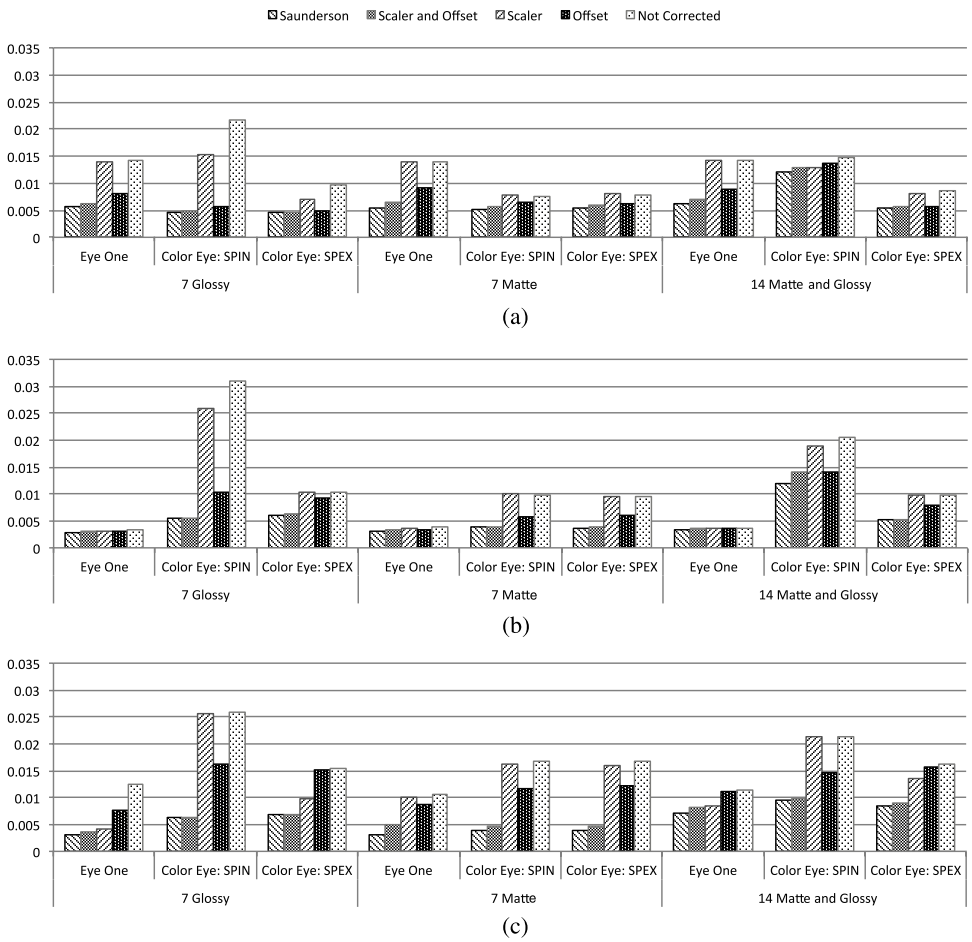

Figure 7. Average RMS values of corrected and measured reflectance factors by different spectrophotometers and the PR-655 in different lighting geometries for 14 gray patches. (a) Diffuse lighting, (b) 45°/0°-dual lights, (c) 45°/0°-single light.

geometry. This implies that the specular reflectances are smaller for camera-capturing geometries, even compared to di:8° geometry. This explains why di:8° yielded larger errors for all the geometries when no correction was applied.

Comparing matte and glossy patches, glossy patches were more sensitive to the geometrical changes. This sensitivity can be either amplified or weakened according to the capturing geometries. For example, diffuse or 45°/0°-dual light geometry with matte patches gave small and similar RMS values regardless of the spectrophotometer geometry. In contrast, glossy patches in the 45°/0°-single-light condition led to distinct results for different spectrophotometric geometries.

The surface correction resulted in almost the same RMS values for all of the capturing geometries (plotted as *Saunderson* bars in Fig. 7). For the diffuse capturing geometry, the RMS values were slightly larger, which could be caused by lower illumination level in the diffuse capturing geometry. The results indicate that the Saunderson correction is capable of eliminating the effect of geometric differences. The *Scaler* and *Offset* bars in Fig. 7 correspond to Eq. (5). This method yielded similar RMS values as the Saunderson correction method, confirming the validity of the assumption made. This also implies that a characterization method with a 3×4 transformation matrix (by adding the offset coefficients in the regression model) is capable of improving the estimations compared to a 3×3 matrix, but only for certain materials; this is evaluated in the next phase of the experiment.

Neither the single scaler method nor the single offset method performed satisfactorily in compensating for the geometrical changes. The single offset correction (indicated by the *Offset* bars in Fig. 7) is particularly effective for the Color-Eye 7000 spectrophotometer with SPIN; nevertheless, the RMS errors are still large for some geometries. Likewise, the single scaler correction (indicated by the *Scaler* bars in Fig. 7) could not noticeably address geometrical changes.

It is also important to mention that a single set of the Saunderson coefficients is valid only for either matte or glossy samples; so combinations of matte and glossy samples should not be used for deriving the coefficients or optimizing the transformation matrix. In other words, the optimized k values are different for matte and glossy samples because of their surface properties. Accordingly, k values optimized for glossy patches cannot be used for matte samples, and vice versa. This dissimilarity resulted in greater RMS errors when both matte and glossy patches were utilized for optimization (look at Fig. 7 when 14 matte and glossy samples are utilized).

In summary, the measured reflectance factors are different according to the surface properties of the samples

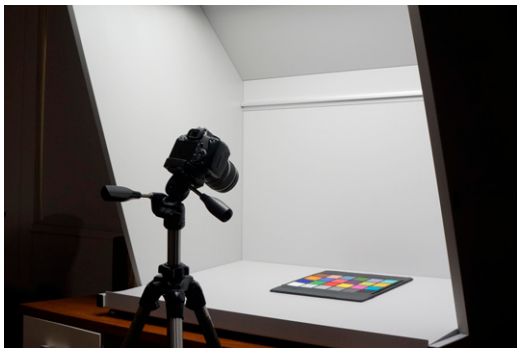

Figure 8. Lighting and capturing setups using a digital camera (phase II).

and the geometry of the measurements. Also, the reflectance factor geometrical mismatches can be corrected for a given capturing geometry using the Saunderson equation and minimizing the spectral RMS values. The conclusions drawn in this phase were used for characterizing a trichromatic camera in the second phase of the experiment.

Phase II

A Canon Rebel XSi digital SLR camera with EF-S 17-85 mm $f/4.0$–5.6 IS lens was selected to evaluate the profiling process. The PR-655 in the diffuse lighting geometry of the first phase (corresponding to Fig. 5(a)) along with the Xrite Eye-one spectrophotometer were selected as spectral measurement instruments for this phase. The camera-taking geometry was similar to the diffuse lighting condition of phase I, illustrated in Figure 8. The Xrite Eye-one spectrophotometer was chosen due to ease of measurements, and the diffuse geometry was chosen to be different from the Xrite Eye-one spectrophotometer geometry. The images were captured in RAW format (CR2) with a 12-megapixel resolution and converted to 16-bit Tiff format to be processed in Matlab R2010b.

The exposure time and aperture size of the camera were adjusted (with an ISO of 100) so as to be in the dynamic range of the camera. The linearity of the camera sensor was evaluated by taking several shots with different exposure times of a uniform field when no lens was installed.

Flat-field and dark current/optical flare corrections were applied to the taken images in advance of any further processes. The dark current and optical flare of the camera were extracted by placing a light trap in each scene. We used a light trap made for dark calibration of the Color-Eye 7000 spectrophotometer, shown in Figure 9. Since the optical flare is variable from scene to scene, the optical flare and dark current correction were done for each image. Afterward, the collected images were rectified for lighting nonuniformities and lens fall-off using a flat uniform surface of fluorilon (with the surface close to that of a Lambertian), known as flat-field correction.

The RGB responses of each color patch were extracted by averaging the pixel values. Since the distance between the camera and the color targets are different according to the capturing geometry, a different number of pixels was averaged for each geometry by considering approximately

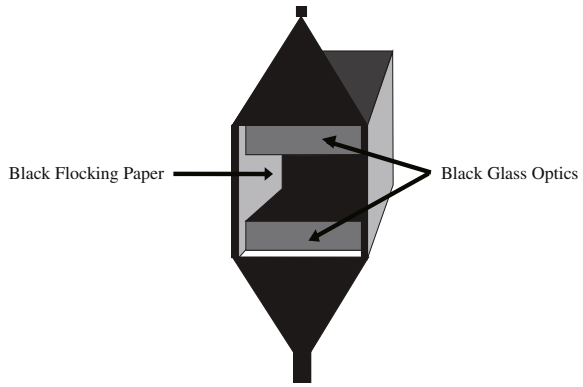

Figure 9. Light trap for measuring dark current and flare [ColorEye® 7000A manual, www.xrite.com].

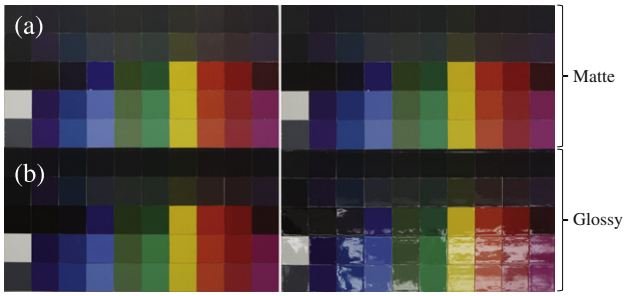

Figure 10. The custom color chart with 100 glossy and matte patches under the light booth at specular angle. (a) 50 matte patches, (b) 50 glossy patches. The image at the left corresponds with the isotropic lighting. The image on the right shows the same color chart in the specular angle under the light booth for illustrating the difference between glossy and matte patches.

50% of the sample area from its center. A ColorChecker SG (*SG*), an Xrite ColorChecker Classic (*Classic*), and a custom color target (*CC*) were used for evaluations. In contrast to the ColorChecker Classic with matte surfaces, the ColorChecker SG has semi-gloss patches. We only evaluated 24 color patches of the SG corresponding to the ColorChecker Classic so two color charts can be compared according to their surface properties.

The custom color chart was comprised of 100 matte and glossy patches. Different patches were made by mixing GOLDEN Matte Fluid Acrylic paints to achieve a reasonable color gamut, a set of neutral and dark patches, as shown in Figure 10. An automotive gloss coating was applied to half of the samples to generate the glossy surfaces (Fig. 10(b)). Each of the color charts was used as a training color target, and the transformation matrix was investigated by estimating the tristimulus values of the custom color chart for the 1931 standard observer and standard illuminant D65 based on spectral measurements using the PR-655. The training and test color charts information is provided in Table I. Five characterization methods were examined for camera characterization based on conventional linear and surface-corrected methods.

Results of Phase II

The resulting RMS values of ΔE_{XYZ} and CIEDE2000 are shown in Figure 11. As already mentioned, five characteri-

Table I. Training and test data for evaluating color characterization methods.

Geometry Code	Training Data	Testing Data
Classic	24 patches of the ColorChecker Classic	
SG	24 patches of the ColorChecker SG	
Custom All	100 patches of the custom color chart	100 patches of custom color chart
Custom-Matte	50 matte patches of the custom color chart	
Custom-Glossy	50 glossy patches of the custom color chart	
Total	148 patches including 24 patches of the Color Checker Classic, 25 patches of the ColorChecker SG and 100 patches of custom color chart	

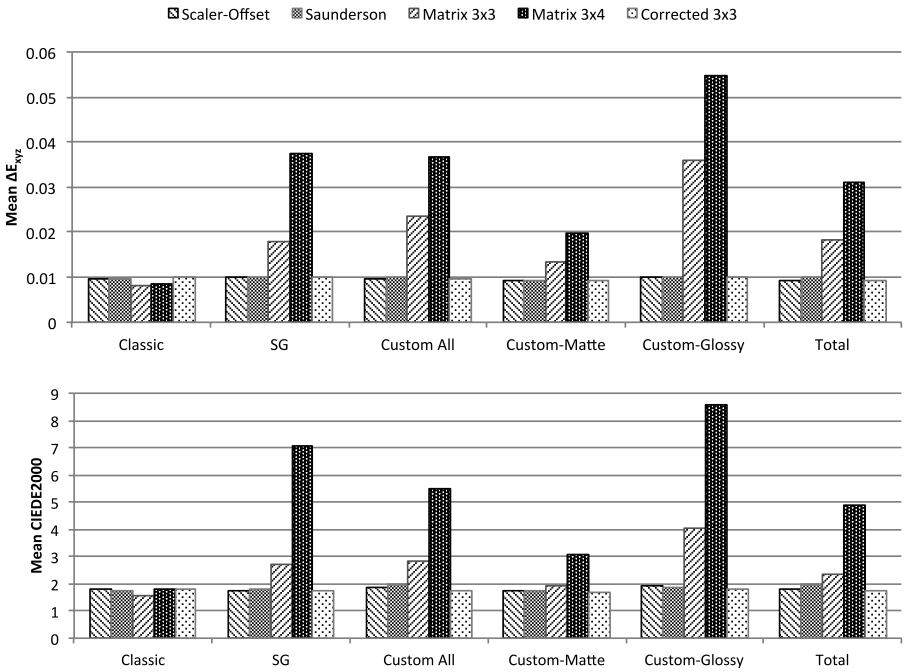

Figure 11. Comparison of mean value of ΔE_{xyz} (top) and CIEDE2000 (bottom) for regular and optimized reflectance factors of 100 patches of the custom color chart. The horizontal axis specifies the color checker used for training the algorithm, according to Table I.

zation methods were evaluated for camera characterization. The first and second methods were based on the optimization of the reflectance factors by the simplified and basic forms of the Saunderson equation, denoted as *Scaler-Offset* and *Saunderson*, respectively, in Fig. 11. The third and fourth methods converted RGB camera signals to colorimetric values by means of a conventional 3 × 3 and 3 × 4 transformation matrices (denoted as *Matrix* 3 × 3 and *Matrix* 3 × 4 in Fig. 11). Finally, the fifth method was a Saunderson-based 3 × 3 matrix derived according the correction made on the 3 × 4 matrix and Eq. (11), shown as *Corrected* 3 × 3 in Fig. 11.

According to Fig. 11, the Saunderson-based methods enhanced the process compared to typical 3 × 3 and 3 × 4 transformation matrices. Using the ColorChecker Classic as the training data resulted in the smallest color difference for typical characterization methods due to its matte surface. The scaler-offset method, with the assumption of the equality of k_2 for both geometries, had identical performance for all color checkers and about similar performance to the Saunderson correction method, as expected, considering the results from the previous phase. Looking at the RMS and CIEDE2000 values in Fig. 11, results for the new corrected matrix (*corrected* 3 × 3 method) are also comparable to those from the Saunderson and scaler-offset methods, which shows that the procedure of optimizing the 3 × 3 matrix can be followed by the simplification explained in Eqs. (6) and (13) rather than nonlinear optimization algorithms.

When color charts other than the ColorChecker Classic were used as a training data set, typical characterization methods (with no surface correction) led to noticeably large errors (particularly for glossy and semi-glossy color targets). One of the extreme cases it to use ColorChecker SG as the training data set with the considerable differences in measured reflectance factors among geometries. Estimated and actual CIELAB values of 100 test patches of the custom color chart (for diffuse image-capturing geometry and spectral data measured by the Eye-one spectrophotometer), and using the ColorChecker SG as the training chart, are plotted in Figure 12(a). Since diffuse lighting conditions cause the color patches to appear lighter and more desaturated for the ColorChecker SG patches, the 3 × 4 transformation matrix compensates the color changes by shifting the color values toward darker and more chromatic

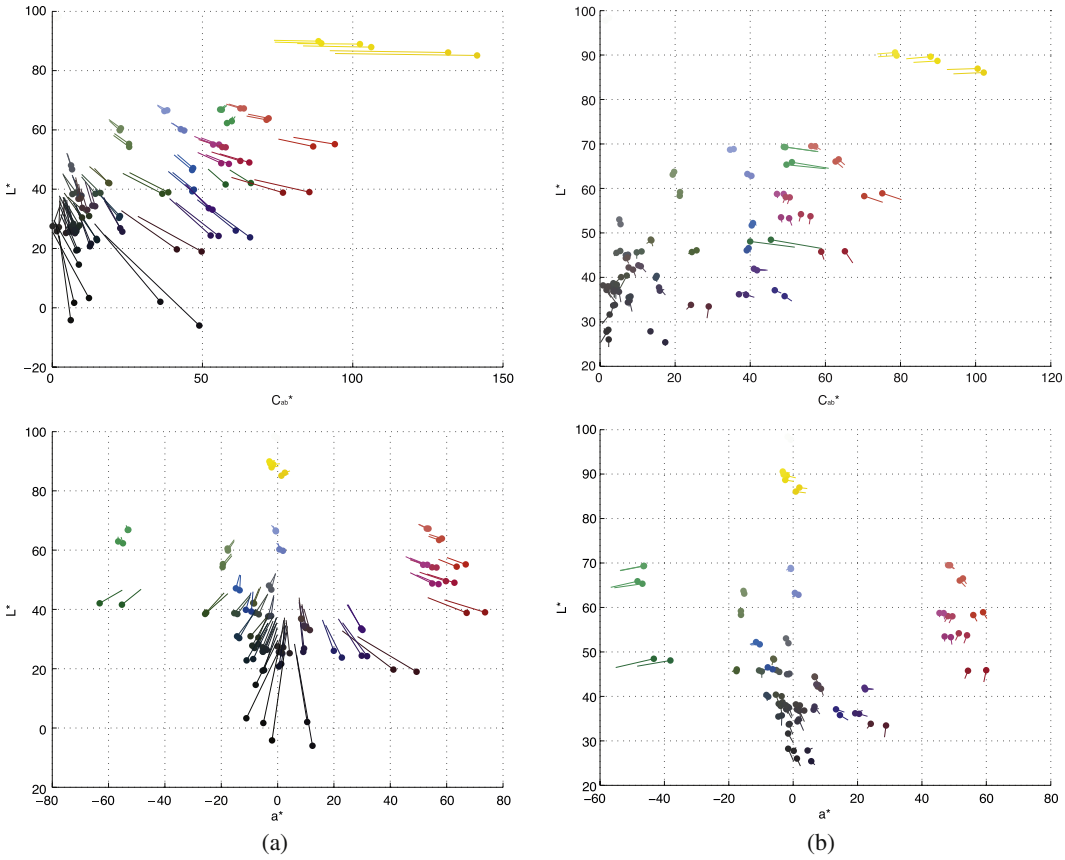

Figure 12. CIELAB values of the custom color chart patches produced by a conventional 3 × 4 transformation matrix (a) and the Saunderson-based (b) methods in CIELAB color space (a*–L* and C*–L*). In each plot, filled circles represent estimated values of the custom color chart. The line connected to each circle shows the location of the actual value measured by the PR-655. These plots correspond to diffuse image-capturing geometry and spectral measurements by the Eye-one spectrophotometer.

regions. However, obviously this transformation is not valid for glossy and matte samples, because their color appearance changes differently. Therefore, the transformation matrix is considered a geometric-dependent matrix that is only suitable for the semi-glossy samples of the ColorChecker SG. Conversely, Saunderson correction methods tended to reduce the RMS error, independent of the training data set, because the radiance data corresponded to the scene geometry. The improvement in estimation when the ColorChecker SG was used is shown in Fig. 12(b). Note that the correction specifically had better predictions, particularly for dark samples, after Saunderson-based corrections.

Using the same dataset for testing and training did not make an efficient improvement to the performance of the Saunderson-based models. This highlights that the algorithm did not overfit to the training data, showing independence from the training color target. It is important to point out that one source of estimation error is a result of differences between the camera sensor spectral sensitivities and the human visual system. This source of the error has been studied and mentioned by previous researchers.[8] There are other sources of error, such as nonuniformity of the detector and color patches, and camera and spectrophotometer noise levels, which limit characterization algorithms to a maximum achievable accuracy.

The optimized Saunderson-based 3 × 3 transformation matrix (Corrected 3 × 3) and regular method matrices (3 × 4 and 3 × 3 matrices) are shown in Table II. Using the Saunderson surface correction, the 3 × 3 matrices were almost similar for all color charts and the training data, whereas the regular method using a 3 × 4 matrix resulted in different matrix values, particularly for the offset row. Note that, when the ColorChecker Classic was used as the training data set, the offset values were close to zero, and the transformation matrix was close to a 3 × 3 matrix. The offset values for the ColorChecker SG and glossy samples of the custom color chart were larger compared to other training data sets, illustrating their sensitivity to the geometric changes. A conventional 3 × 3 matrix is quite different according to different color targets, indicating the dependence on the training data.

The optimized Saunderson coefficients from two capturing geometries of this phase are summarized in Table III. According to the optimized coefficients, k_{ins} is rather similar for the two spectral measurement geometries when the ColorChecker Classic was used as the training data set, because its appearance changes in similar fashion for both geometries. For other training sets, k_{ins} for the spectrophotometers were smaller than those for the spectral radiance measurements. The Eye-one spectrophotometer

Table II. The transformation matrices from different methods.

Training data	Corrected 3 × 3			Matrix 3 × 3			Matrix 3 × 4		
	1.77	0.63	0.18	1.73	0.57	0.14	1.79	0.66	0.18
24 patches of the ColorChecker Classic	0.21	2.50	−1.18	0.24	2.51	−1.10	0.19	2.46	−1.14
	0.63	−0.45	5.44	0.59	−0.47	5.31	0.67	−0.39	5.37
							−0.01	−0.01	−0.01
	1.77	0.63	0.20	1.60	0.39	−0.10	1.89	0.68	0.22
24 patches of the ColorChecker SG	0.15	2.44	−1.22	0.38	2.78	−1.01	0.14	2.53	−1.28
	0.71	−0.36	5.48	0.37	−0.76	5.30	0.78	−0.34	5.76
							−0.05	−0.06	−0.06
	1.74	0.60	0.12	1.68	0.53	0.04	1.75	0.61	0.13
50 matte patches of the custom color chart	0.27	2.52	−0.99	0.33	2.59	−0.93	0.28	2.54	−0.99
	0.62	−0.41	5.27	0.38	−0.67	5.01	0.61	−0.42	5.30
							−0.02	−0.03	−0.03
	1.80	0.64	0.17	1.58	0.46	−0.02	1.74	0.63	0.17
50 glossy patches of custom color chart	0.16	2.47	−1.08	0.27	2.48	−0.91	0.16	2.37	−1.03
	0.66	−0.39	5.30	0.16	−0.88	4.54	0.65	−0.37	5.09
							−0.05	−0.05	−0.06

Table III. Optimized Saunderson coefficients in different capturing geometries.

	Spectrophotometer geometry (Eye-one)			Camera-taking geometry (diffuse)		
	k_1	k_2	k_{ins}	k_1	k_2	k_{ins}
Classic	0.04	0.63	0.30	0.07	0.61	0.24
SG	0.03	0.60	0.27	0.10	0.59	0.57
Custom-Matte	0.04	0.61	0.29	0.07	0.59	0.50
Custom-Glossy	0.07	0.60	0.00	0.05	0.59	1.00

detects smaller amounts of specular reflectance compared to the diffuse camera-taking geometry. However, as already mentioned, the optimized coefficients are relative values and do not express absolute physical metrics.

As a conclusion, the application of typical 3 × 4 matrix-based methods (without surface correction) is limited to the specific materials as the training color target. Correcting for the surface mismatches, the camera signals are converted to the tristimulus values of scene geometry rather than the spectrophotometer geometry. These corrections make the characterization valid for all of the materials in the scene. Comparing Saunderson-based methods, the classic Saunderson equation is preferred for more accurate results, but it is more expensive computationally.

The ability of the scalar-offset method in characterizing isotropic surface properties is also applicable for evaluating the characterization process when spectroradiometric data are not available. According to the results, the tristimulus values of the spectrophotometer can be obtained from the RGB responses using the $\boldsymbol{M}_{4*3}$ in Eq. (6). The differences between estimated and measured tristimulus values of the training dataset can be utilized for examining the performance of the transformations. Obviously, this transformation matrix is merely valid for surfaces similar to the training color patches.

Phase III

The last phase of the experiment considered the independence of the characterization models. In this phase,

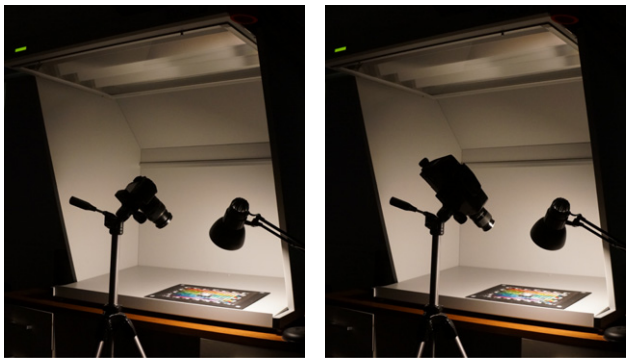

(a) (b)

Figure 13. Lighting and capturing setups for measuring by the digital camera (a) and the PR-655 (b) used for the third phase of the experiment.

the transformation matrix optimized in phase II was used to estimate the radiance values of ten patches of the ColorChecker DC in a directional lighting condition shown in Figure 13. The evaluation patches contained five glossy and five matte patches (Figure 14).

The new illumination geometry and color patches were completely different to those used for the camera characterization. However, the camera exposure time and aperture size were identical to the training condition.

The spectral radiance of the samples in the new geometry was measured using the PR-655 and converted to tristimulus values under D65 using the spectral radiance of PTFE. Since the goal is to evaluate the characterization method according to the incoming radiance (but not training the model), flat-field correction was unnecessary in this phase. Other sources of error, such as lens fall-off for the new geometry, still exist and cause minor color differences. The workflow of calculating the new tristimulus values relative to those from the characterized camera is illustrated in Figure 15. The upper part of the diagram illustrates the workflow of the camera characterization, which actually explains the previous phase. In the evaluation section, the radiometric

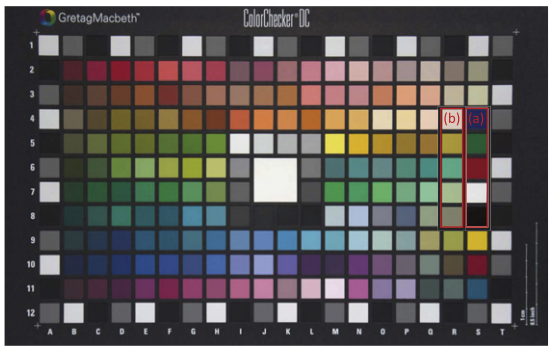

Figure 14. The ColorChecker DC Evaluation patches: (a) five glossy patches, (b) five matte patches.

values from the PR-655 should be converted to tristimulus values comparable to the characterization step. Therefore, radiometric values were converted to relative reflectance using the spectral radiance of PTFE under the source lighting condition (diffuse lighting under the light booth in the second phase). The calculated tristimulus values from the PR-655 and characterized camera were evaluated using the CIEDE2000 color difference formula.

Results of Phase III

The mean and maximum CIEDE2000 and ΔE_{xyz} RMS values for the ten samples of the ColorChecker DC are shown in Table IV. The average CIEDE2000 value for the surface-corrected methods is approximately 2.6 with color patches made from consistent materials (i.e. either all matte or all glossy). However, it should be noted that, even for the color charts with the uniform surface properties, the illumination and capturing geometry must be identical for all the patches when they are used for the characterization. This is one of the factors that makes working with glossy samples difficult, because their appearances are more sensitive to spatial changes due to specular reflectances. Over and above these restrictions, the camera characterization process would be independent of the color chart used as the training dataset.

The regular characterization methods (3 × 4 matrix and 3 × 3 matrix) produced the largest color differences. A paired-sample t-test on the ΔE_{xyz} RMS values also confirmed that the 3 × 4 matrix produced larger errors in all cases (95% significance level). The conventional 3 × 3 matrix led to the second largest error except when the ColorChecker Classic was used for training because of the large variances of ΔE_{xyz} values. For conventional matrix-based methods, the best matches resulted with the ColorChecker Classic. In contrast, glossy and semi-glossy samples resulted in the poorest results, specifically for the 3 × 4 matrix transformation. However, even using the ColorChecker Classic with matte samples did not lead to smaller color differences than any of the surface-corrected methods.

Looking at Table IV, the CIEDE2000 values of Saunderson-based methods (e.g. Scaler-Offset, Saunderson, and Corrected 3 × 3) are similar for different training data, which implies independence to both the geometry and the training data. The estimation error increased slightly when a combination of training data with different surface properties was utilized, as expected. Another possible source of error in the new geometry is the illumination level, which is lower than in the calibration geometry. This affects the signal-to-noise ratio (SNR) and sensor linearity for both the spectroradiometer and camera measurements, particularly for short wavelengths. The use of an incandescent light source also intensifies the deviations, because of lower radiance in short wavelengths. The maximum error for this geometry occurred for the glossy red sample in all cases. Considering the large amount of absorption in the middle and short wavelengths for the glossy red patch, the incandescent light source, and the lower illumination level, any measurement uncertainty propagates to large estimation errors.

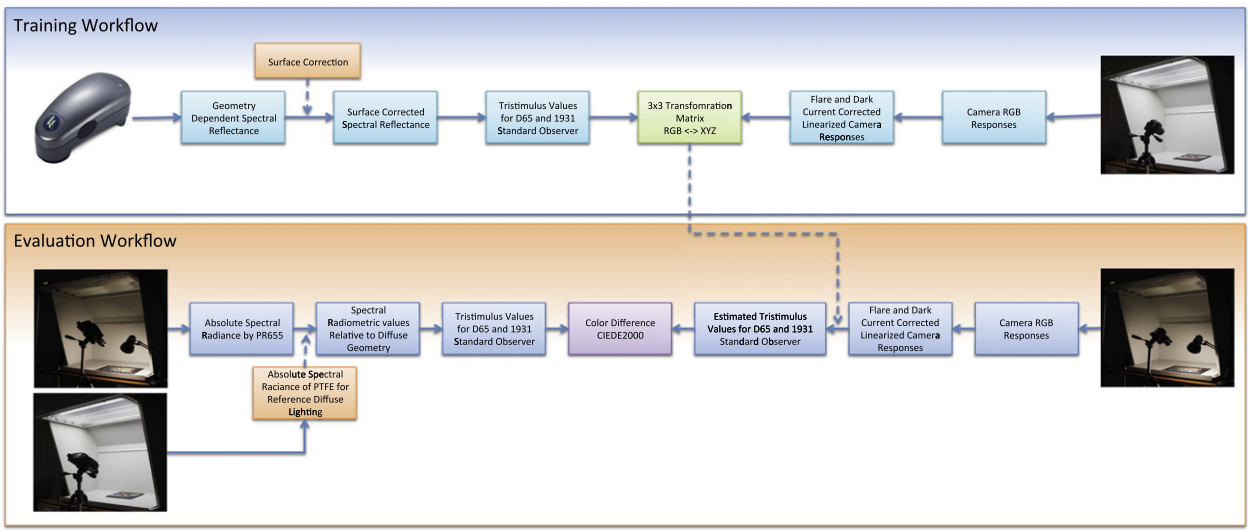

Figure 15. Workflow of training and evaluating the performance of the characterization algorithm for different lighting geometry.

Table IV. Mean and maximum values of ΔE_{xyz} RMS and CIEDE2000 of the third phase for the five glossy and five matte patches of the ColorChecker DC.

		Scaler-Offset		Saunderson		Matrix 3 × 3		Matrix 3 × 4		Corrected 3 × 3	
	Training Dataset	Mean	Max	Mean	Max	Mean	Max	Mean	Max	Mean	Max
ΔE_{xyz} RMS	Classic	0.0052	0.0190	0.0051	0.0188	0.0074	0.0154	0.0111	0.0150	0.0051	0.0198
	SG	0.0060	0.0166	0.0058	0.0189	0.0182	0.0534	0.0474	0.0559	0.0060	0.0199
	Custom All	0.0060	0.0179	0.0068	0.0182	0.0200	0.0585	0.0420	0.0493	0.0054	0.0181
	Custom-Matte	0.0054	0.0159	0.0057	0.0156	0.0124	0.0337	0.0255	0.0316	0.0057	0.0161
	Custom-Glossy	0.0055	0.0200	0.0052	0.0200	0.0277	0.0831	0.0586	0.0705	0.0053	0.0202
	Total	0.0055	0.0167	0.0068	0.0181	0.0167	0.0485	0.0378	0.0441	0.0058	0.0172
CIEDE2000	Classic	2.4	8.1	2.3	8	2.5	7.1	3.7	7.3	2.4	7.8
	SG	2.4	7	2.4	8.3	3.3	8	13	26	2.7	8.7
	Custom All	2.7	7.7	3	8.1	3.2	4.8	10.1	19	2.6	7.3
	Custom-Matte	2.5	6.4	2.5	6.6	2.7	4.4	6.7	13.1	2.6	6.8
	Custom-Glossy	2.6	8.1	2.4	7.8	3.9	6.4	13.7	24.4	2.5	7.8
	Total	2.5	7.2	3	8.2	2.9	4.6	9.5	18.4	2.6	7.6

CONCLUSIONS

In this research, a geometrically independent camera characterization workflow was introduced by modeling the appearance of the training data set due to geometrical changes. A surface correction method based on the Saunderson equation was selected and applied to the spectral data of the training data set to compensate for geometrical dissimilarities between camera responses and reflectance factors provided by spectrophotometers. The Saunderson equation takes the advantage of simplicity and applicability for isotropic paint surfaces compared to the variety of available models.

The proposed method was evaluated in three phases. In the first phase, the influence of the Saunderson correction was assessed by comparing spectrophotometric and spectroradiometric measurements. The correlation of the reflectance factors from two spectrophotometers and a spectroradiometer was studied in three lighting geometries. The results of this phase validated that the Saunderson correction method was capable of compensating for appearance changes due to lighting geometries. In addition, a simplified version of the Saunderson equation was also implemented and evaluated, assuming similarity in the internal reflection coefficient for different geometries. The trivial differences between the Saunderson equation and the simplified form of the equation confirmed the validity of this assumption for paint surfaces.

In the second phase of the experiment, the Saunderson correction was used in the color characterization of a DSC. Three different color charts were used for training the characterization algorithms to estimate the tristimulus values of a test color chart containing glossy and matte patches. From the different color charts, the ColorChecker Classic led to the best results when no correction was applied to the reflectance factors, because of its Lambertian-like surface properties. As a result, matte surfaces are more appropriate for color characterization of the camera when no further processes are applied to the reflectance factors. New algorithms corrected the reflectance factor for geometric changes and eliminated dependences on the lighting geometries and training target materials.

Finally, the characterized camera, using training datasets under a diffuse geometry, was used to predict the tristimulus values of a series of matte and glossy samples of a distinct color chart (ColorChecker DC) and a directional lighting geometry. New characterization workflows resulted in acceptable color difference values compared to conventional 3 × 3 and 3 × 4 transformation matrices. Comparing generated matrices from conventional characterization methods, greater color differences were achieved because of over-fitting the colorimetric coordinates for the spectrophotometric geometry. The best results were obtained for conventional characterization methods when the ColorChecker Classic was used as the training dataset, even though the color difference errors were still larger than in Saunderson-based models.

ACKNOWLEDGMENT

This work was supported by a grant from the Andrew W. Mellon Foundation.

APPENDIX A

This appendix includes mathematical steps for deriving Eq. (4) from Eq. (3).

Equation (3) can be rewritten as follows:

$$R_{m,c} = \frac{(1-k_1)(1-k_2)R_m - (1-k_1)(1-k_2)k'_{ins}k'_1}{(1-k'_1)(1-k'_2) - k'_{ins}k'_1k'_2 + k'_{ins}k'_1k_2 + R_m(k_2-k'_2) + k_{ins}k_1} \tag{14}$$

or

$$R_{m,c} = \frac{R_m + \frac{DC+E}{DB-A}}{\frac{B}{DB-A}R_m + \frac{C}{DB-A}}, \tag{15}$$

where A, B, C, D, and E are defined as

$$A = (1-k_1)(1-k_2) \tag{16}$$

$$B = (k_2 - k_2') \tag{17}$$

$$C = (1 - k_1')(1 - k_2') - k_{ins}' k_1' k_2' + k_{ins}' k_1 k_2 \tag{18}$$

$$D = k_{ins} k_1 \tag{19}$$

$$E = (1 - k_1)(1 - k_2) k_{ins}' k_1'. \tag{20}$$

By defining further auxiliary variables, the following equation is derived:

$$R_m' = \frac{R_m + \alpha}{\beta R_m + \gamma}, \tag{21}$$

where $\alpha = \frac{DC+E}{DB-A}$, $\beta = \frac{B}{DB-A}$, $\gamma = \frac{C}{DB-A}$.

APPENDIX B

This appendix shows the mathematical steps for deriving Eq. (5).

By letting k_2 be equal to k_2' in Eq. (3),

$$R_{m,c} = \frac{(1 - k_1)(1 - k_2) R_m - (1 - k_1)(1 - k_2) k_{ins}' k_1'}{(1 - k_1')(1 - k_2') - k_{ins}' k_1' k_2' + k_{ins}' k_1' k_2' + R_m (k_2 - k_2')} + k_{ins} k_1; \tag{22}$$

then

$$R_{m,c} = \frac{(1 - k_1) R_m - (1 - k_1) k_{ins}' k_1'}{(1 - k_1')} + k_{ins} k_1. \tag{23}$$

By reforming this equation based on variable R_m, the following equation is obtained:

$$R_{m,c} = \left(\frac{1 - k_1}{1 - k_1'} \right) R_m + k_{ins} k_1 - \left(\frac{1 - k_1}{1 - k_1'} \right) k_{ins}' k_1', \tag{24}$$

which is similar to the equation below:

$$R_{m,c} = \mu R_m + \rho, \tag{25}$$

where $\mu = \left(\frac{1-k_1}{1-k_1'} \right)$ and $\rho = + k_{ins} k_1 - \left(\frac{1-k_1}{1-k_1'} \right) k_{ins}' k_1'$.

APPENDIX C

The following is a list of procedures for deriving the transformation matrix for colorimetric camera characterization according to the new method. The transformation is based on camera responses of a light trap (RGB_k), a flat-field image from a uniform diffuse surface (RGB_{fl}), RGB values of a reference white (RGB_w) with the corresponding average reflectance (R_w), and average RGB values of each patch of the color target (RGB_{cc}). All the RGB values must be scaled between zero and unity. The characterization process can be summarized as follows.

1. Subtract RGB_k from RGB_w and RGB_{cc}. RGB_k also can be the RGB values correlated to the light trap for each scene independently by placing the light trap in all the scenes. However, since the lighting and camera position do not change during the characterization procedure, RGB_k is likely to be similar for all the scenes. All RGB images are supposed to be flare/black current corrected hereafter.
2. For flat fielding, multiply each of pixels of the color target image to the corresponding pixel of R_w/RGB_{fl}.
3. Extract the RGB values for each sample of the color target by averaging a reasonable number of pixels from the color target RGB image (RGB_{cc}).
4. Calculate the $\boldsymbol{M}_{3\times4}$ matrix according to the averaged RGB values of the color target image and corresponding spectrophotometric *XYZ* values for a desired viewing condition:

$$\boldsymbol{M}_{3*4} = \begin{bmatrix} X_m \\ Y_m \\ Z_m \end{bmatrix}_{3*n} \begin{bmatrix} R \\ G \\ B \\ 1 \end{bmatrix}^{+}, \tag{26}$$

   where the superscript + refers to the pseudo-inverse of the matrix $\boldsymbol{A}$, which is equal to $(A^T A)^{-1} A^T$.
5. Omit the offset column (the fourth column) of matrix $\boldsymbol{M}_{3*4}$ to obtain a 3×3 matrix, M'.
6. Optimize the scalar value, μ, using RGB_w values from the camera:

$$\mu = \left(\boldsymbol{M}_{3*3}' \begin{bmatrix} R_w \\ G_w \\ B_w \end{bmatrix}_{3*1} \right)^{+} \begin{bmatrix} X_{il} \\ Y_{il} \\ Z_{il} \end{bmatrix}_{3*1}, \tag{27}$$

   where X_{il}, Y_{il}, and Z_{il} are the tristimulus values of the chosen light source.
7. Calculate the final transformation matrix by multiplying the optimized scalar and the 3×3 matrix from step 2:

$$\boldsymbol{M}_{cr} = \mu \boldsymbol{M}_{3*3}'. \tag{28}$$

8. Convert the RGB values of any images by the camera to tristimulus values by multiplying the RGB values by the transformation matrix $\boldsymbol{M}_{cr}$. Each image taken should already be corrected for flare and dark current by subtracting the RGB values of the light trap for each scene.

REFERENCES

[1] P. Green and L. W. MacDonald, *Colour Engineering: Achieving Device Independent Colour* (John Wiley & Sons Inc., New York, 2002), chs. 6 and 8.

[2] G. Sharma and R. Bala, *Digital Color Imaging Handbook* (CRC, Boca Raton, FL, 2003), ch. 5.

[3] M. Fairchild, *Color Appearance Models*, 2nd ed. (John Wiley & Sons Ltd, West Sussex, England, 2005), ch. 19.

[4] S. Westland, C. Ripamonti, and J. Wiley, *Computational Colour Science using MATLAB* (John Wiley & Sons Ltd, West Sussex, England, 2004), ch. 8.

[5] G. Hong, M. R. Luo, and P. A. Rhodes, "A study of digital camera colorimetric characterisation based on polynomial modelling," Color Res. Appl. **26**, 76–84 (2001).

[6] M. D. Fairchild, D. R. Wyble, and G. M. Johnson, "Matching image color from different cameras," Proc. SPIE **6808**, 10 (2008).

[7] V. Cheung, S. Westland, D. Connah, and C. Ripamonti, "A comparative study of the characterisation of colour cameras by means of neural networks and polynomial transforms," Coloration Technol. **120**, 19–25 (2004).
[8] F. M. Martínez Verdú, J. Pujol Ramo, and P. Capilla Perea, "Characterization of a digital camera as an absolute tristimulus colorimeter," J. Imaging Sci. Technol. **47**, 279–295 (2003).
[9] K. Barnard and B. Funt, "Camera characterization for color research," Color Res. Appl. **27**, 152–163 (2002).
[10] V. Cheung, S. Westland, and M. Thomson, "Accurate estimation of the nonlinearity of input/output response for color cameras," Color Res. Appl. **29**, 406–412 (2004).
[11] C. Li, G. Cui, and M. R. Luo, "The accuracy of polynomial models for characterising digital cameras," *Proc. AIC Interim. Meet Colour Communication and Management* (Bangkok, 2003), pp. 166–170.
[12] T. Cheung and S. Westland, "Color selections for characterization charts," *Proc. IS&T's CGIV 2004 Second European Conf. on Colour in Graphics, Imaging, and Vision* (IS&T, Springfield, VA 2004), pp. 116–119.
[13] D. Nyström, "Colorimetric and multispectral image acquisition using model-based and empirical device characterization," *Proc. Image Analysis, 15th Scandinavian Conference, SCIA 2007* (Denmark, 2007), pp. 798–807.
[14] ISO 17321-2006 *Graphic Technology and Photography: Colour Characterisation of Digital Still Cameras (DSCs) Part 1*, (ISO, Geneva), www.iso.org.
[15] P. Green and M. Kriss, *Color Management: Understanding and Using ICC Profiles* (John Wiley & Sons Ltd, West Sussex, United Kingdom, 2010), ch. 14.
[16] H. R. Kang, *Computational Color Technology* (Society of Photo Optical, Bellingham, Washington, 2006), ch. 8.
[17] ISO 13655-2009 *Graphic Technology: Spectral Measurement and Colorimetric Computation for Graphic Arts Images*, (ISO, Geneva), www.iso.org.
[18] R. Berns, *Billmeyer and Saltzman's Principles of Color Technology* (John Wiley and Sons, Danvers, MA, 2000), ch. 1.4.
[19] P. M. Hubel, J. Holm, G. D. Finlayson, and M. S. Drew, "Matrix calculations for digital photography," *Proc. IS&T/SID Fifth Color Imaging Conf. Color Science, Systems and Applications* (IS&T, Springfield, VA, 1997), pp. 105–111.
[20] J. Dorsey, H. Rushmeier, and F. Sillion, *Digital Modeling of Material Appearance* (Morgan Kaufmann, Burlington, MA, 2008), ch. 5.
[21] G. J. Ward, "Measuring and modeling anisotropic reflection," *Proc. SIGGRAPH'92 Proc. of the 19th Annual Conf. on Computer Graphics and Interactive Techniques* (New York, 1992), pp. 265–272.
[22] J. Saunderson, "Calculation of the color of pigmented plastics," J. Opt. Soc. Am. A **32**, 727–729 (1942).
[23] H. G. Völz, *Industrial Color Testing* (Willey-VCH, New York, 1995), ch. 3.
[24] R. McDonald, *Colour Physics for Industry* (Society of Dyers and Colourists, West Yorkshire, England, 1987), ch. 6.
[25] J. Ryde, "The scattering of light by turbid media. Part I," Proc. R. Soc. Lond. Ser. A **131**, 451–464 (1931).
[26] J. Ryde and B. Cooper, "The Scattering of light by turbid media. Part II," Proc. R. Soc. Lond. Ser. A **131**, 464–475 (1931).
[27] M. M. G. D. Finlayson, "Root-polynomial colour correction," *Proc. IS&T/SID Nineteenth Imaging Conf.* (IS&T, Springfield, VA 2011), pp. 115–119.
[28] R. McDonald, *Colour Physics for Industry*, 2nd ed. (Society of Dyers and Colourists, West Yorkshire, England, 1997), ch. 6.